EPR study of Ni^+ centers in $CsCaF_3$

B. Villacampa, R. Alcalá, and P. J. Alonso
Instituto de Ciencia de Materiales de Aragón, Facultad de Ciencias, Universidad de Zaragoza-Consejo Superior de Investigaciones Científicas, Plaza de S. Francisco s/n, E-50009 Zaragoza, Spain

M. Moreno
DCITTYM, Sección de Materiales, Facultad de Ciencias, Universidad de Cantabria, E-39005 Santander, Spain

M. T. Barriuso
Departamento de Física Moderna, Facultad de Ciencias, Universidad de Cantabria, E-39005 Santander, Spain

J. A. Aramburu
DCITTYM, Sección de Materiales, Facultad de Ciencias, Universidad de Cantabria, E-39005 Santander, Spain
(Received 19 March 1993; revised manuscript received 6 July 1993)

Ni^+ centers produced by room-temperature x-ray irradiation of $CsCaF_3$ single crystals have been studied by EPR. Three types of centers have been detected, all of them with tetragonal symmetry and the $|x^2-y^2\rangle$ ground state. The models for these centers, which are similar to those observed in other fluoride crystals, consist of a Ni^+ ion surrounded by a Jahn-Teller elongated fluorine octahedron [Ni^+(I)] and the same model, but with one and two nearest-neighbor fluorine vacancies, for Ni^+(II) and Ni^+(III). The spin-Hamiltonian parameters (g and superhyperfine tensors) have been measured and compared with the values predicted from molecular-orbitals calculations of the NiF_6^{5-} and NiF_4^{3-} complexes. The results allow us to determine the values of the Ni^+-F^- distances. An anomalous behavior is found for Ni^+(I). The orthorhombic character of the superhyperfine interaction with the equatorial fluorines also has been theoretically estimated and is in good agreement with the experimental results. Besides, an explanation based on the spin polarization of filled orbitals has been proposed to account for the superhyperfine interaction with the axial fluorines. Dynamical effects observed between 20 and 30 K in the Ni^+(I) EPR signal have been discussed on the basis of a dynamical Jahn-Teller effect.

I. INTRODUCTION

The spectroscopic properties of Ni^{2+} ions in octahedral environments have been extensively studied[1-5] both because of their basic interest and because Ni^{2+}-doped crystals have potential applications as active media in ionic solid-state lasers. Much less information is available on the spectroscopy of nickel ions in other unusual charge states such as Ni^+. They can be produced by irradiation with ionizing radiations of crystals containing Ni^{2+} ions, but their concentration is usually too low to detect them by optical techniques.

Electron paramagnetic resonance (EPR) measurements allow the detection of Ni^+ ions and provide information on its ground state,[6-9] which is orbitally degenerate in an octahedral environment and can be split by Jahn-Teller (JT) interaction. Usually a static tetragonal JT distortion is observed at low temperatures. In octahedral fluoride environments two types of distortions have been reported.[7-9] In one of them, observed by Hayes and Wilkens[7] in LiF and NaF, a compression of the octahedron along one of the fourfold axes is found and this leaves the $|3z^2-r^2\rangle$ orbital as the ground state. However, recent data[10,11] indicate that the assignment of these centers to Ni^+ ions can be wrong. The other distortion corresponds to an elongated octahedron and, in this case, the ground state is the $|x^2-y^2\rangle$. Together with the JT distorted ones, other tetragonal Ni^+ centers with the $|x^2-y^2\rangle$ ground state have been detected by EPR in x-ray-irradiated fluoride crystals doped with Ni^{2+}.[7-9] In these cases the tetragonal distortion is due to the presence of one or two F^- nearest-neighbor vacancies to the Ni^+ ion.

Besides the qualitative models for the different centers it is interesting to have some quantitative estimation of the relaxation of F^- ions surrounding the Ni^+. This can be achieved by a careful analysis of the EPR results. In some recent papers, the spin-Hamiltonian (SH) parameters [g tensor ([g]) and superhyperfine (SHF) tensor] of NiF_6^{5-} and NiF_4^{3-} units and their dependence on the Ni^+-F^- distances along the tetragonal axis (R_{ax}) and perpendicular to this axis (R_{eq}), have been calculated using different methods.[12-15] These calculations allow the estimation of the Ni^+-F^- distances from the experimental values of those parameters. This procedure has already been applied to Ni^+ centers in different matrices and the distances derived from the experimental values of different SH parameters have proved to be consistent. However, when the Ni^+-F^- distance increases there are some deviations that should be checked by putting the Ni^+ centers in other matrices where that distance is larger. On the other hand, some dynamical effects are expected for the JT Ni^+ centers which, to our knowledge, have not been clearly detected and which could be favored by the increase of the Ni^+-F^- distance.

0163-1829/94/49(2)/1039(9)/$06.00

Because of this we have undertaken the EPR study of Ni^+ centers in $CsCaF_3$. Three different types of tetragonal Ni^+ centers have been observed. Models are proposed for these centers and the values of the components of their g and SHF tensors have been obtained and discussed as a function of the Ni^+-F^- distance following the theoretical treatments reported in the literature. The thermal evolution of the EPR signal of one of these centers has also been studied and a qualitative discussion in terms of a dynamical JT effect is given.

II. EXPERIMENT

Nickel-doped $CsCaF_3$ crystals were grown by the Bridgman technique. The Ni content of the starting materials ranged from 0.1 to 1 mol%. X-ray irradiations were performed using a Cu-target x-ray tube working at 40 kV and 20 mA. EPR measurements were taken in a Varian E-112 spectrometer working in the x band. The low-temperature spectra were taken with either a continuous flow helium cryostat (ESR-900 from Oxford Instruments) or a liquid-nitrogen quartz immersion Dewar. Magnetic-field values were determined with a Bruker ER035M nuclear magnetic resonance (NMR) Gauss meter and the diphenylpicrylhydrazyl (DPPH) resonance line ($g = 2.0037 \pm 0.0002$) was used to calibrate the microwave frequency.

Thermal annealings were performed in air keeping the samples for 30 min at the desired temperature and slowly cooling down to room temperature (RT) to prevent stresses induced by thermal quenching. A 150 W high-pressure Xe lamp was used for optical bleaching.

III. EXPERIMENTAL RESULTS

The EPR spectrum of "as-grown" Ni-doped $CsCaF_3$ crystals shows the signal corresponding to Ni^{2+} ions in an octahedral environment. After RT x-ray irradiation, new signals due to different types of Ni^+ ions have been observed. It is worth mentioning here that a similar irradiation of $CsCdF_3$ crystals showing a similar Ni^{2+} signal does not produce Ni^+ ions in concentrations detectable in our EPR measurements. The results corresponding to $CsCaF_3$ are the following.

Besides the Ni^{2+} signal, the EPR spectrum of a RT x-ray-irradiated $CsCaF_3$:Ni crystal measured at liquid-nitrogen temperature (LNT) with the magnetic field **B** parallel to a $\langle 100 \rangle$ direction shows two patterns in the $g \sim 2.7$ (~ 245 mT) and $g \sim 2.1$ (~ 315 mT) regions (see Fig. 1). Measuring at higher temperatures, these patterns broaden and become undetectable at about 300 K. This spectrum is very similar to those previously reported in other fluoroperovskites,[8,9] where these two patterns have been associated with tetragonal Ni^+ centers. The pattern at low field ($g \sim 2.7$) corresponds to centers with the tetragonal axis parallel to the applied magnetic field, while the high-field one ($g \sim 2.1$) is due to centers with the tetragonal axis perpendicular to **B**.

The low-field pattern (parallel centers) contains two groups of strongly overlapped lines. From the analogy with the results in $KMgF_3$ (Ref. 8) and $RbCaF_3$ (Ref. 9),

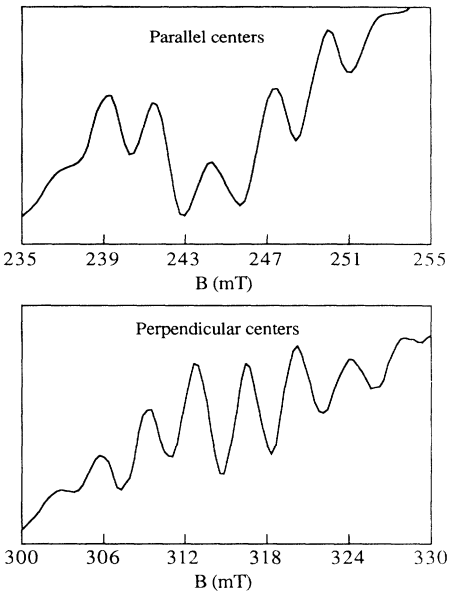

FIG. 1. EPR spectrum of Ni^+ centers in x-ray-irradiated $CsCaF_3$. Measured at LNT with $\mathbf{B} \| \langle 100 \rangle$.

we propose that each of the groups is formed by five lines with relative intensities following the sequence 1:4:6:4:1 due to a SHF interaction with four fluorine nuclei in the plane perpendicular to the C_4 axis (equatorial fluorines) that are equivalent for this orientation of the magnetic field. The g values corresponding to the central line of each of the two groups are ~ 2.74 and ~ 2.68, respectively. The peak to peak width of the lines at lower fields is about 1.3 mT while that of the higher field lines is about 1 mT. The relative intensities of the two groups of lines can be changed by heating the RT-irradiated crystals up to 500 K in such a way that the group of lines at higher fields decreases with respect to that at lower fields (spectrum a in Fig. 2). On the other hand, illuminating the irradiated samples with the light of a Xe lamp, the signal at higher fields increases with respect to the other one (spectrum b in Fig. 2). Taking advantage of these results it has been possible to separate the signals corresponding to the two types of centers. On heating at temperatures higher than 750 K, both signals disappear. By similarity with the results in $KMgF_3$ and $RbCaF_3$, the centers responsible for these signals will be labeled Ni^+(II) and Ni^+(III), respectively.

The high-field region ($g \sim 2.1$), associated with centers having their tetragonal axis perpendicular to the applied magnetic field, shows a complicated SHF structure which is due to a superposition of the contributions from Ni^+(II) and Ni^+(III) centers. These two contributions can be separated in the way indicated above (see Fig. 2). The spectrum of each of the centers consists of seven lines with an approximate intensity ratio 1:2:3:4:3:2:1. This structure is due to the interaction with the four equatorial fluorines, being the interaction constant with two of them, approximately one-half of the interaction constant corresponding to the other two.

A rotational diagram of each of the Ni^+(II) and

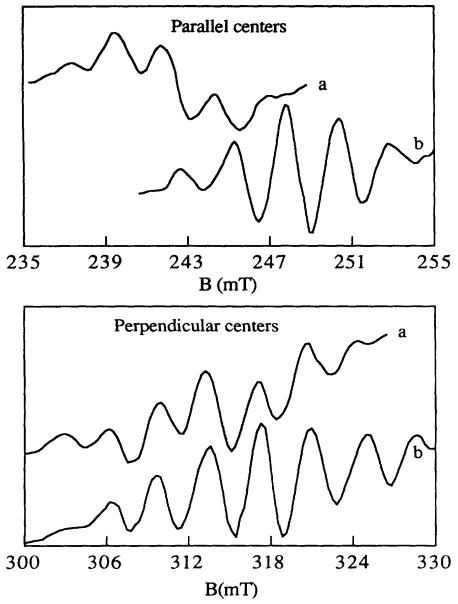

FIG. 2. EPR spectrum of Ni^+ centers types II and III: (a) Ni^+(II) obtained by heating a RT irradiated sample up to 500 K, (b) Ni^+(III) obtained by optical bleaching of a RT-irradiated sample. Measured at LNT with $\mathbf{B}\|\langle 100\rangle$.

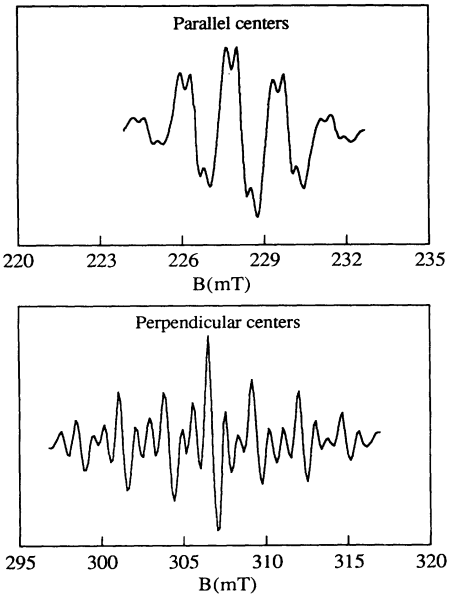

FIG. 3. EPR spectrum of Ni^+(I) centers. Measured at 15 K with $\mathbf{B}\|\langle 100\rangle$.

Ni^+(III) signals has been measured at LNT. The positions of the EPR lines can be described using the following SH:

$$H=\beta_e[g_\perp(S_xB_x+S_yB_y)+g_\parallel S_zB_z] + \sum_{j=1}^{4}(A_xS_{x_j}I^j_{x_j}+A_yS_{y_j}I^j_{y_j}+A_zS_{z_j}I^j_{z_j}), \quad (1)$$

where β_e is the Bohr magneton, $S=\frac{1}{2}$ and $I_j=\frac{1}{2}$. The z axis is chosen along the C_4 axis of the defect and the x and y axes are along the $\langle 100\rangle$ directions perpendicular to this tetragonal axis. The z_j axis is along the bonding directions between the Ni^+ ions and the fluorine nuclei that coincide with the $\langle 100\rangle$ directions perpendicular to the tetragonal axis and the x_j axes are parallel to the C_4 direction. By fitting the line positions, calculated using Eq. (1), to the observed ones, the SH parameters given in Table I have been obtained.

If the crystal irradiated at RT is measured at temperatures below 35 K, another EPR signal similar to those of Ni^+(II) and Ni^+(III) centers is observed. This signal becomes dominant at low temperatures. We have plotted in Fig. 3 the spectrum measured at 15 K with the applied magnetic field **B** parallel to a $\langle 100\rangle$ direction. The centers responsible for it will be labeled Ni^+(I) and the rotational diagram measured with **B** rotating in a (001) plane shows that they also have tetragonal symmetry.

The spectrum plotted in Fig. 3 can be understood in a similar way to that of Ni^+(II) and Ni^+(III) centers. The low-field part is due to centers with the tetragonal axis parallel to the applied magnetic **B** and is formed by five groups of three lines with an intensity ratio 1:4:6:4:1 among the five groups and a ratio 1:2:1 within each group. This structure is due to a SHF interaction with two groups of four and two F^{19} nuclei, the fluorines within each group being equivalent for this magnetic-field orientation.

The high-field part of the spectrum corresponds to centers with the tetragonal axis perpendicular to **B**. The SHF structure consists of seven groups of three lines each, the relative intensities of the groups being in the approximate ratio 1:2:3:4:3:2:1, while the three lines of each group are again in the ratio 1:2:1. This structure is due to the interaction with three groups of two equivalent F^{19} nuclei, being one of the two larger interaction constants one-half of the other.

The positions of the lines corresponding to the rotational diagram of the Ni^+(I) centers can be obtained using the SH given by Eq. (1), adding the term,

$$\sum_{i=1}^{2}[A'_\perp(S_xI^i_x+S_yI^i_y)+A'_\parallel S_zI^i_z], \quad (2)$$

with $I^i=\frac{1}{2}$ and where $A'_\parallel$ and $A'_\perp$ are the components of the SHF tensor giving the interaction with the two axial fluorines. The SH parameters obtained by fitting the calculated positions to the observed ones are given in Table I.

We have also measured the evolution of the Ni^+(I) EPR spectrum with temperature between 15 and 30 K.

TABLE I. Spin-Hamiltonian parameters for Ni^+ centers in $CsCaF_3$. Superhyperfine constants are given in $\times 10^{-4}$ cm^{-1}. Primed values correspond to the interaction with the two axial fluorines.

$CsCaF_3$	$g_\parallel$	$g_\perp$	A_x	A_y	A_z	$A'_\parallel$	$A'_\perp$
Ni^+(I)	2.892(2)	2.142(2)	23(2)	27(2)	54(2)	6(1)	10(1)
Ni^+(II)	2.740(2)	2.116(2)	30(2)	35(2)	70(2)		
Ni^+(III)	2.676(2)	2.089(2)	32(2)	37(2)	75(2)		

The results obtained with the magnetic field parallel to a $\langle 100 \rangle$ direction are given in Fig. 4. It can be seen that the parallel signal (low field) shows a simultaneous broadening of each of five groups of lines but keeping the same height ratios.

On the other hand, the behavior observed in the perpendicular signal (high field) is more complicated. The relative heights and widths of the different lines change between 15 and 30 K. In particular, if we consider the seven main lines (labeled 1 to 7 in Fig. 4), the heights of the odd lines decrease more strongly than those of the even ones. At temperatures higher than 35 K all the lines broaden and disappear.

IV. DISCUSSION

Ni^{2+} ions enter $CsCaF_3$ in a Ca^{2+} site surrounded by an octahedron of fluorines. They can be transformed to Ni^+ by trapping electrons produced during x-ray irradiation. At the same time anion vacancies, also produced by irradiation, can be associated with some of the Ni^+ ions to compensate for its effective negative charge, giving place to different types of perturbed Ni^+ centers.

Ni^+ ions have a $3d^9$ electronic configuration. It is known that these ions placed in an octahedral environment experience a tetragonal Jahn-Teller (JT) distortion that raises the degeneracy of the ground-state doublet (^2E_g).[16] For static distortions it is found that when the octahedron is elongated along one of the fourfold axes, the $|x^2-y^2\rangle$ state has the lowest energy while with a compression, the $|3z^2-r^2\rangle$ state is the lowest one.

EPR measurements allow one to distinguish between these two situations. It has been shown[16] that if the $|x^2-y^2\rangle$ is the ground state, the components of $[g]$ should follow the relation $g_\parallel > g_\perp > 2$, while if the unpaired electron is in the $|3z^2-r^2\rangle$ oribtal, the relation is $g_\perp > g_\parallel \sim 2$. In our case it is clear that in all our Ni^+ centers the ground state is the $|x^2-y^2\rangle$. This behavior is similar to that reported in other fluoroperovskites.[8,9]

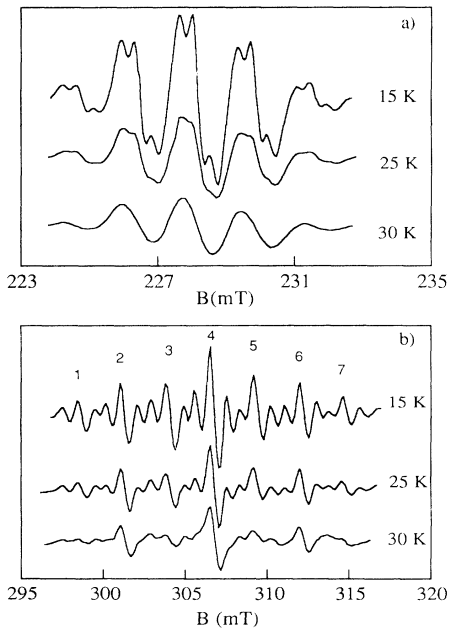

FIG. 4. Thermal evolution of the Ni^+(I) signal: (a) parallel centers and (b) perpendicular centers. Measured with $\mathbf{B} \| \langle 100 \rangle$.

With respect to the different types of Ni^+ centers observed, the models that we propose to account for our results are the following. Ni^+(I) consists of a Ni^+ ion in the center of a JT elongated fluorine octahedron. This explains the observed SHF interaction with two groups of four and two equivalent fluorine nuclei. In the case of Ni^+(II) and Ni^+(III) only the SHF interactions with the four equatorial fluorines are resolved but the width of the lines due to Ni^+(II) is larger than that of Ni^+(III). Besides, the Ni^+(III) center's concentration increases with respect to that of Ni^+(II) by optical bleaching. Taking all this into account and the results previously reported for similar centers in $KMgF_3$ and $RbCaF_3$, we propose for Ni^+(II) and Ni^+(III) a model similar to that of Ni^+(I) but with one and two nearest-neighbor fluorine vacancies, respectively, placed along the tetragonal axis. In the case of Ni^+(II) an unresolved SHF interaction with the remaining axial fluorine would be the reason for the lines being broader than for Ni^+(III). On the other hand, fluorine vacancies produced by ionization of F centers during bleaching can be trapped at Ni^+(I) and Ni^+(II) to give a final increase of the concentration of Ni^+(III). The decrease in the splitting due to the interaction with the axial fluorine in the case of Ni^+(II) with respect to that observed in Ni^+(I) where split lines are resolved, could be understood if in Ni^+(II) centers the Ni^+ ion, due to its effective negative charge, moves away from the axial fluorine toward the vacancy. We have tried to determine a possible displacement of the Ni^+ ion from the plane of equatorial fluorines by means of the rotational diagram of the Ni^+(II) ions but the intensity of the signal was low and we have not been able to detect any clear effect due to this displacement of the Ni^+.

We will analyze now the values of the SH parameters corresponding to the Ni^+ defects. As the thermal evolution of the spectrum shown in Fig. 4 is hardly understood without taking into account dynamic effects, we will begin with a discussion of some of the spin-Hamiltonian parameters that can be explained with a static model and will consider the dynamical behavior afterward.

Thus, in a first step we shall derive the R_{eq} values of the three Ni^+ centers in $CsCaF_3$, using for this goal the experimental isotropic SHF constant A_S corresponding to equatorial ligands. Further, we shall try to explain the microscopic origin of the following aspects. (i) Differences between the $[g]$ tensors corresponding to Ni^+(I) and Ni^+(III) centers. (ii) Dependence of $g_\parallel - g_0$ (g_0 is the electronic g factor) and $g_\perp - g_0$ on R_{eq} for both Ni^+(I) and Ni^+(III) centers along the full fluoroperovskites series. (iii) Orthorhombicity of the SHF tensor for such centers. We do not include explicitly Ni^+(II) centers in this discussion as the corresponding experimental values lie always between those for Ni^+(I) and Ni^+(III).[8,9,13]

The present analysis is partially based on previous work on Ni^+ in fluorides,[15] showing that the properties

of Ni^+(I), Ni^+(II), and Ni^+(III) centers can theoretically be understood to a large extent on the basis of NiF_6^{5-}, NiF_5^{4-}, and NiF_4^{3-} complexes, respectively. Furthermore, the differences exhibited by the SH parameters of a given type of Ni^+ center but placed in different host lattices have reasonably been ascribed to the dependence of the equilibrium distances R_{eq} and R_{ax} on the chemical pressure exerted by the host lattice upon the complex.[8,9,12–15]

For achieving a good understanding of all data concerning Ni^+(I) and Ni^+(III) centers in fluoroperovskites we have performed additional molecular-orbital (MO) calculations of NiF_6^{5-} and NiF_4^{3-} complexes for R_{eq} lying in the range 2.20–2.35 Å. For this goal we have also used two different methods: the local-density functional method multiple scattering $X\alpha$(MSXα)[17] and the semiempirical self-consistent charge extended Hückel (SCCEH) method.[18] In the case of the elongated NiF_6^{5-}, complex calculations have been done for values of R_{ax} equal to 2.33 and 2.43 Å. As explained in Refs. 14 and 15, some calculations have been performed embedding the referred clusters in the simple LiF lattice in order to verify that the electronic properties of Ni^+ centers in fluorides can be explained to a large extent only on the basis of complexes like NiF_6^{5-} and NiF_4^{3-}. More details on calculations are given in Refs. 14 and 15 where results in the domain 2.00 Å $< R_{eq} <$ 2.20 Å were already reported.

In order to clarify the following discussions, it is convenient to now write the normalized wave functions of three relevant orbitals like $b_{1g}^*(\sim|x^2-y^2\rangle)$ (where the unpaired electron is placed), $b_{2g}^*(\sim|xy\rangle)$, and $e_g^*(\sim|xz\rangle,|yz\rangle)$ which determine the SHF and $[g]$ tensors.[19] Such wave functions can be briefly written as follows:

$$\begin{aligned}
|b_{1g}^*\rangle &= \alpha_0|x^2-y^2\rangle-\beta_0|\chi_L^0\rangle\ ,\\
|b_{2g}^*\rangle &= \alpha_1|xy\rangle-\beta_1|\chi_L^0\rangle\ ,\\
|e_g^a a\rangle &= \alpha_2|xz\rangle-\beta_2|\chi_L^{2a}\rangle\ ,\\
|e_g^* b\rangle &= \alpha_2|yz\rangle-\beta_2|\chi_L^{2b}\rangle\ ,
\end{aligned} \tag{3}$$

where $|\chi_L^0\rangle$, $|\chi_L^1\rangle$, $|\chi_L^{2a}\rangle$, and $|\chi_L^{2b}\rangle$ are suitable linear combinations of atomic orbitals (LCAO's) involving ligand orbitals. Among the three b_{1g}^*, b_{2g}^*, and e_g^* levels, only in b_{1g}^* does the ligand 2s-2p hybridization exists and so $|\chi_L^0\rangle$ can be written as

$$\begin{aligned}
|\chi_L^0\rangle &= \mu_p|\chi_{p\sigma}\rangle+\mu_s|\chi_s\rangle\ ,\\
\mu_p^2+\mu_s^2 &= 1\ ,
\end{aligned} \tag{4}$$

where $|\chi_{p\sigma}\rangle$ and $|\chi_s\rangle$ involve LCAO's of 2$p\sigma$ and 2s ligand orbitals, respectively.

The energies of the $b_{2g}^*\rightarrow b_{1g}^*$, and $e_g^*\rightarrow b_{1g}^*$ excitations, which play an important role for understanding the $[g]$ tensor, will be denoted henceforth as Δ_1 and Δ_2, respectively. The transition $a_{1g}^*\rightarrow b_{1g}^*$ involving the remaining antibonding level a_{1g}^* $(\sim|3z^2-r^2\rangle)$ plays, however, a practically negligible role, as all matrix elements of the form $\langle a_{1g}^*|\mathbf{L}|b_{1g}^*\rangle$ are zero.

Let us now first focus on the experimental isotropic SHF constant of equatorial ligands A_s and its relation with R_{eq}. In a good first approximation A_s can be taken as $(A_x+A_y+A_z)/3$ and thus the relation between A_s and $\beta_0\mu_s$ can be written[7,16] as

$$\begin{aligned}
A_s &= A_{2s}^0\beta_0^2\mu_s^2/4\ ,\\
A_{2s}^0 &= (8\pi/3)g_0g_N\beta_e\beta_N|\phi_{2s}(0)|^2\ ,
\end{aligned} \tag{5}$$

where g_N is the nuclear g factor of the ligand, β_N the nuclear magneton, $\phi_{2s}(0)$ the wave function of the 2s orbital of fluorine at the nucleus, and $A_{2s}^0 = 1520\times10^{-4}$ cm^{-1} correspond to the free F^- ion.

As pointed out in Ref. 12, the theoretical results for complexes like NiF_6^{5-} or MnF_6^{4-} indicate that $\beta_0\mu_s$ is given by the law,

$$\beta_0\mu_s = cS_s\ , \tag{6}$$

where $S_s=\langle x^2-y^2|\chi_s\rangle$ is the corresponding group-overlap integral and c is a constant.

As for NiF_6^{5-}, it has been found[15] $S_s^2(R_{eq})\alpha R_{eq}^{-7}$; Eqs. (5) and (6) thus explain the strong dependence of A_s upon R_{eq}.

In applying Eqs. (5) and (6) to relate the experimental A_s value with R_{eq}, S_s can be written in terms of the $\langle 2s|d\sigma\rangle$ diatomic overlap integral between the 2s fluorine orbital and the $d\sigma$ Ni^+ orbital as follows:

$$S_s=\sqrt{3}\langle 2s|d\sigma\rangle\ . \tag{7}$$

The overlap integral can be obtained using the Clementi and Roetti atomic wave functions[20] and depends on R_{eq}. So Eqs. (5) and (6) provide a relationship between the experimental A_s values and R_{eq}. The c constant that takes into account covalency effects has been taken to be $c=1.1$, as for Ni^+ in other similar fluoride environments.[12–15,21] Although the exact value of the c constant is not known for the present case, it is worth stressing here that variations of such a constant alter the R_{eq} value derived from Eqs. (5) and (6) but not the differences among R_{eq} values corresponding to a given center embedded in different host lattices. The values of R_{eq} obtained in this way are 2.27 Å for Ni^+(I), 2.19 Å for Ni^+(II), and 2.17 Å for Ni^+(III). These values are larger than those obtained in $KMgF_3$ and $RbCaF_3$, as expected, because of the larger value of the lattice parameter of $CsCaF_3$. We want to point out that the increase in R_{eq} going from Ni^+(III) and Ni^+(II) to Ni^+(I) is much larger in $CsCaF_3$ than in the other fluoroperovskites.

Let us now discuss the $[g]$ tensor which can be computed once the electronic levels and MO coefficients like α_0, α_1, α_2, etc., are known from MSXα and SCCEH calculations. The expressions relating $g_\parallel$ and $g_\perp$ with the MO coefficients and energy levels of tetragonal complexes involving d^9 ions are well explained in Ref. 19.

In Fig. 5 the theoretical dependence of $g_\parallel-g_0$ and $g_\perp-g_0$ upon R_{eq} found for both NiF_6^{5-} and NiF_4^{3-} complexes is displayed. It can be noticed that the MSXα and the SCCEH methods both give rise to a similar dependence of $g_\parallel$ and $g_\perp$ on R_{eq}. Let us write the depen-

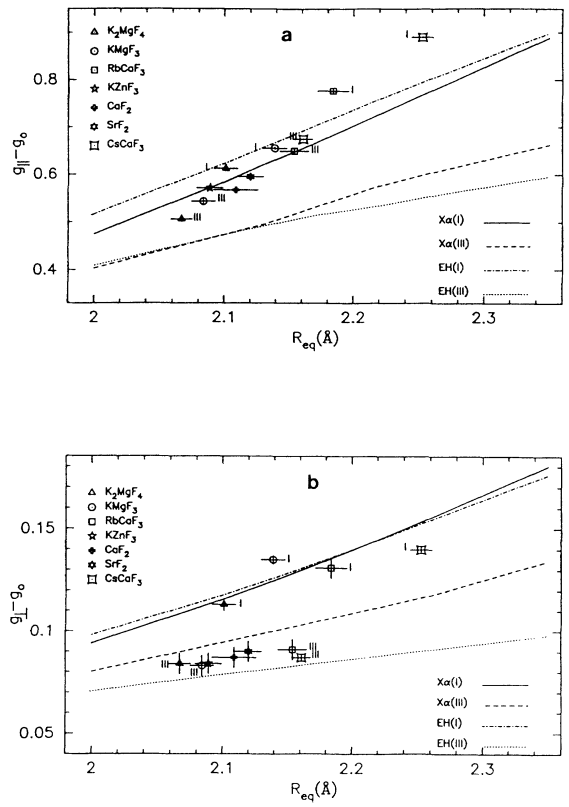

FIG. 5. Theoretical variation of (a) $g_{\parallel}-g_0$ and (b) $g_{\perp}-g_0$ calculated through MSXα and SCCEH methods for NiF_4^{3-} and NiF_6^{5-} complexes. Experimental points for Ni^+(I) and Ni^+(III) centers in fluoroperovskites as well as for the nearly square planar NiF_4^{3-} centers formed in CaF_2 and SrF_2 are also shown. The R_{eq} values have been derived from the experimental SHF tensor using Eqs. (5) to (7).

dence on R_{eq} of a quantity Q (like Δ_1^{-1}, Δ_2^{-1}, $g_{\parallel}-g_0$, or $g_{\perp}-g_0$) in the vicinity ($\Delta R_{eq}/R_{eq}<0.1$) of $R_{eq}=2.15$ Å as $Q\alpha R_{eq}^{-n}$ (of the same type as the one in the crystal-field approximation where $n=5$). From the performed calculations for different R_{eq} values, the obtained values of the exponents n are gathered in Table II. It is worth remembering here that in the case of the SCCEH method, the values of such exponents are very sensitive to the quality of the employed wave functions.[15] So if single-zeta wave functions are used instead of the much more realistic Clementi-Roetti wave functions, it is found, for instance, that $\Delta_1\alpha R_{eq}^{-8}$ for NiF_6^{5-} that has to be compared with $\Delta_1\alpha R_{eq}^{-4.4}$ derived from Table II. It can be noticed that (i) the exponent found for $g_{\parallel}-g_0$ ($g_{\perp}-g_0$) is a little smaller than that for $\Delta_1^{-1}(\Delta_2^{-1})$ and (ii) the value $n=1.6$, found through the SCCEH method for $g_{\perp}-g_0$ for Ni^+(III), is especially low, thus predicting a very slight dependence of $g_{\perp}-g_0$ on R_{eq} for this kind of center.

TABLE II. Assuming a dependence $Q\alpha R_{eq}^{-n}$ for a given quantity Q, the values of the exponent n corresponding to the six mentioned parameters for Ni^+(I) and Ni^+(III) centers are collected in this table. For each parameter and center, two values of n are given, coming from SCCEH (upper value) and MSXα (lower value) calculations, respectively. The values for Ni^+(I) center have been calculated for $R_{ax}=2.45$ Å.

Center	$g_{\parallel}-g_0$	$\Delta^2 g_{\parallel}$(CF)	Δ_1^{-1}	$g_{\perp}-g_0$	$\Delta^2 g_{\perp}$(CF)	Δ_2^{-1}
I	3.6	4.2	4.4	3.7	4.8	4.9
	4.5	4.6	4.7	4.6	5.7	5.2
III	2.7	2.6	3.8	1.6	2.5	3.5
	3.7	4.0	4.1	3.5	4.3	4.2

These results can partially be understood by having in mind the microscopic origin of $[g]$. For the present case, the theoretical expressions for $g_{\parallel}-g_0$ and $g_{\perp}-g_0$ can be briefly written as[19]

$$\begin{aligned} g_{\parallel}-g_0&=\Delta^2 g_{\parallel}(\mathrm{CF})+\Delta^3 g_{\parallel}(\mathrm{CF}) ,\\ g_{\perp}-g_0&=\Delta^2 g_{\perp}(\mathrm{CF})+\Delta^3 g_{\perp}(\mathrm{CF}) , \end{aligned} \tag{8}$$

where $\Delta^2 g$ and $\Delta^3 g$ mean the second- and third-order contributions to $[g]$ and CF stands for crystal field. Because of the high ionicity of the present complexes, the contribution of charge-transfer excitation to $[g]$ can be fully ignored, although it is very important in strongly covalent d^9 complexes,[22] such as $AgBr_6^{4-}$, where $g_{\perp}$ is practically equal to $g_{\parallel}$. Therefore, in the present cases only the contributions arising from crystal-field (CF) excitations are considered.

The expressions for $\Delta^2 g_{\parallel}$(CF) and $\Delta^2 g_{\perp}$(CF) can simply be written as

$$\begin{aligned} \Delta^2 g_{\parallel}(\mathrm{CF})&=(8\xi_M/\Delta_1)f_1(\alpha_0,\alpha_1,\mu_p,\xi_L) ,\\ \Delta^2 g_{\perp}(\mathrm{CF})&=(2\xi_M/\Delta_2)f_2(\alpha_0,\alpha_2,\mu_p,\xi_L) , \end{aligned} \tag{9}$$

where ξ_M and ξ_L are the spin-orbit-interaction constants of the metal and the ligand, respectively.

The expressions for f_1 and f_2 acting as reduction factors for low-covalency situations are given in Ref. 19. For the present case, where ionicity is high, the values of f_1 and f_2 are not far from unity ($f_1=0.94; f_2=0.95$) and depend very slightly on R_{eq}. Therefore, the R_{eq} dependence of $\Delta^2 g_{\parallel}$(CF) and $\Delta^2 g_{\perp}$(CF) mimics that of Δ_1^{-1} and Δ_2^{-1}, respectively, to a greater extent. It is worth noting, however, the non-negligible role played by the third-order contributions, especially in the case of the perpendicular component.

The full expressions for $\Delta^3 g_{\parallel}$(CF) and $\Delta^3 g_{\perp}$(CF) in a MO scheme have already been reported.[19] It is worth noting that $\Delta^3 g_{\parallel}$(CF) and $\Delta^3 g_{\perp}$(CF) are both negative, depending on quantities like $(\Delta_1\Delta_2)^{-1}$, Δ_1^{-2}, etc. and so they are more sensitive to R_{eq} changes than $\Delta^2 g_{\parallel}$(CF) and $\Delta^2 g_{\perp}$(CF). Furthermore, although $|\Delta^2 g_{\parallel}(\mathrm{CF})/\Delta^3 g_{\parallel}(\mathrm{CF})|=11$, the ratio $|\Delta^2 g_{\perp}(\mathrm{CF})/\Delta^3 g_{\perp}(\mathrm{CF})|$ is only equal to 3, stressing that third-order corrections are more important for a good understanding of $g_{\perp}-g_0$than for the corresponding to $g_{\parallel}-g_0$. For the sake of clarity, numerical values for the NiF_6^{5-} complex are given in Table III. By virtue of the present arguments we can understand (i) why the dependence $(g_{\parallel}-g_0)\alpha R_{eq}^{+n_1}$ involves an exponent n_1, which is, however, slightly smaller than m_1 appearing in $\Delta_1^{-1}\alpha R_{eq}^{+m_1}$, (ii) why

TABLE III. Values of the different contributions to $g_\parallel - g_0$ and $g_\perp - g_0$ of NiF_6^{5-} obtained using the following parameters derived from a SCCEH calculation: $\Delta_1 = 4700\ cm^{-1}$, $\Delta_2 = 5100\ cm^{-1}$, $\alpha_0 = 0.991$, $\alpha_1 = 0.993$, $\alpha_2 = 0.997$, $\beta_0 = 0.304$, $\beta_1 = 0.218$, $\beta_2 = 0.157$, and $\mu_p = 0.954$. Distances are $R_{eq} = 2.26$ Å and $R_{ax} = 2.43$ Å.

	$\Delta^2 g(CF)$	$\Delta^3 g(CF)$	$\Delta^2 g(CF) + \Delta^3 g(CF)$	Full diagonalization
$g_\parallel - g_0$	0.9136	−0.0939	0.8197	0.8028
$g_\perp - g_0$	0.2141	−0.0619	0.1523	0.1543

$m_1 - n_1$ is smaller than $m_2 - n_2$, where m_2 and n_2 are associated with Δ_2^{-1} and $g_\perp - g_0$.

Let us now compare the theoretical prediction with the experimental $g_\parallel$ and $g_\perp$ values for the three Ni^+ centers in $CsCaF_3$ as well as in other fluoroperovskites. The corresponding R_{eq} values displayed in Fig. 5 have been derived as explained above from the experimental isotropic part of the SHF constant A_s. It can be seen in Fig. 5 that the theoretical predictions for Ni^+(I) and Ni^+(III) centers are not far from the experimental values. This is encouraging since no adjustable parameters have been used in our calculations. In particular, it is shown that the experimental $g_\perp - g_0$ values for Ni^+(III) centers display, in fact, a very slight dependence upon R_{eq}. The measured $g_\perp - g_0$ values for the Ni^+(I), Ni^+(II), and Ni^+(III) centers in $CsCaF_3$ fit reasonably well within the general trends formed for other fluoroperovskites. It can be noted, however, that the predicted $g_\parallel - g_0 = 0.80$ value for $CsCaF_3$:Ni^+(I) is slightly smaller than the experimental one $g_\parallel - g_0 = 0.89$, stressing a small deviation which was previously encountered[15] for $RbCaF_3$:Ni^+(I). This deviation could reflect an exponent $n_1 = 5.5$ which is slightly higher than $n_1 = 4.3$, determined theoretically.

Now it is worth pointing out that the A_s and $g_\parallel$ parameters both indicate an increase of R_{eq} close to 7×10^{-2} Å on passing from $RbCaF_3$:Ni^+(I) to $CsCaF_3$:Ni^+(I). Comparing this value with the increase corresponding to the perfect lattice $\Delta R_0 = 3.8 \times 10^{-2}$ Å, it can be seen that ΔR_{eq} is clearly larger. This is unusual behavior and both theoretical and experimental work involving Ni^+ ions in other fluoroperovskites such as $KZnF_3$ and $KCaF_3$ are in progress trying to understand it.

Looking at the whole series of Ni^+(I) and Ni^+(III) centers in fluoroperovskites, Fig. 5 points out that for a given R_{eq} value, the $g_\parallel$ and $g_\perp$ values for Ni^+(III) are smaller than for Ni^+(I). More precisely, the removal of two axial ligands keeping R_{eq}, induces decrements of ~ 15 and $\sim 30\%$ for $g_\parallel - g_0$ and $g_\perp - g_0$, respectively. Theoretical changes of $\sim 20\%$ are calculated for $g_\parallel - g_0$.

The microscopic origin of these differences between the $[g]$ tensor of Ni^+(I) and Ni^+(III) centers can be explained as follows. Keeping R_{eq}, the removal of two axial ligands in NiF_6^{5-} gives rise to a smaller separation between d levels of Ni^+ and $2p$ levels of equatorial F^- and this induces an increase of Δ_1 and Δ_2, as explained in Ref. 15. Furthermore, in the case of Δ_2, a supplementary increase is produced as the removal of axial ligands also suppresses the bonding with $2p$ levels of axial F^- ions in the e_g^* level and thus decreases its one-electron energy. Bonding with $2p$ levels of axial F^- ions is not possible, however, for b_{1g}^* and b_{2g}^* one-electron orbitals. In order to be more specific, the calculated MSXα values for NiF_6^{5-} corresponding to $R_{eq} = 2.26$ Å and $R_{ax} = 2.43$ Å were $\Delta_1 = 4900\ cm^{-1}$ and $\Delta_2 = 5160\ cm^{-1}$, while they become equal to $\Delta_1 = 5970\ cm^{-1}$ and $\Delta_2 = 6570\ cm^{-1}$ for NiF_4^{3-} computed at the same equatorial distance $R_{eq} = 2.26$ Å.

Before ending this section let us briefly comment on the differences between the present analysis based on a MO description and the results reached through a pure crystal-field description. In fact, Eqs. (6) and (7) do not appear to be very different from those predicted by the pure crystal-field model in cases like the present one, where bonding is highly ionic. This high ionicity ($\beta_0^2 \cong 0.10$, $\beta_1^2 \cong 0.03$, $\beta_2^2 \cong 0.02$ for NiF_6^{5-}) leads to reduction factors f_1 and f_2, which are close to unity as pointed out before. The most remarkable differences between the MO and the pure crystal-field description appears, however, when the calculated values of Δ_1 and Δ_2 transitions are compared. In fact the values obtained through the pure crystal-field model are about four times smaller than those reached through a MO description, the latter ones being consistent with the experimental $[g]$ tensor. A similar situation has been found for O_h complexes involving $3d$ ions where the experimental 10 Dq value is usually five times higher than that calculated through the crystal-field expression.[15]

Let us now comment on the orthorhombic character displayed by the experimental SHF tensor of the three Ni^+ centers found in $CsCaF_3$:Ni^+. Such a character, although compatible with a D_{4d} or C_{4v} point group, has rarely been observed for d^9 impurities in such symmetries. The present data indicate that the "out of the equatorial plane" component A_x is smaller than in the in-plane component A_y. A_x, A_y, and A_z can be expressed as follows:

$$\begin{aligned} A_x &= A_x^1 + A_x^2(\mathrm{CF}) , \\ A_y &= A_y^1 + A_y^2(\mathrm{CF}) , \\ A_z &= A_z^1 + A_z^2(\mathrm{CF}) . \end{aligned} \tag{10}$$

Here A_x^1, A_y^1, A_z^1 are the contributions derived in first-order perturbations given by the well-known expressions,

$$\begin{aligned} A_x^1 &= A_y^1 = A_s - A_p , \\ A_z^1 &= A_s + 2A_p , \end{aligned} \tag{11}$$

where A_s is the isotropic SHF constant defined in Eq. (5) and

$$\begin{aligned} A_p &= A_p^0 \beta_0^2 \mu_p^2 / 4 , \\ A_p^0 &= (2/5) g_0 g_N \beta_e \beta_N \langle r^{-3} \rangle_{2p} \end{aligned} \tag{12}$$

and $\langle r^{-3} \rangle_{2p}$ is the mean value of r^{-3} for a $2p$ fluorine orbital.

Though up to first order, the SHF tensor exhibits an

axial symmetry, the orthorhombic character appears when the second-order contributions are considered. They arise because of the admixture of higher excited states into the ground state due to spin-orbit coupling. The results reported in Ref. 18 are

$$A_x^2(\mathrm{CF}) = -(2/5)(t_1/8 + 3t_2/20\sqrt{2})A_p^0 ,$$
$$A_y^2(\mathrm{CF}) = -(2/5)(3t_1/80 + t_2/2\sqrt{2})A_p^0 , \quad (13)$$

where

$$t_1 = 8\alpha_0\alpha_1\beta_0\beta_1\mu_p q_1(\xi_M/\Delta_1) ,$$
$$t_2 = 2\alpha_0\alpha_2\beta_0\beta_2\mu_p q_2(\xi_M/\Delta_2) , \quad (14)$$
$$q_i = 1 - [\beta_0\beta_i/(\Gamma_i\alpha_0\alpha_i)]\mu_p(\xi_L/\xi_M) \quad (i = 1,2) ,$$

with $\Gamma_1 = 2; \Gamma_2 = \sqrt{2}$.

As for present case, the β_1 and β_2 coefficients involved in the b_{1g}^* and e_g^* π levels are similar and also $\Delta_1 \cong \Delta_2$, therefore we can take as a first approximation $t_1/t_2 = 4$ and then

$$A_x^2(\mathrm{CF}) - A_y^2(\mathrm{CF}) = -(7/200)(1 - 1/\sqrt{2})A_p^0 t_1 . \quad (15)$$

As both $A_x^2(\mathrm{CF})$ and $A_y^2(\mathrm{CF})$ are negative, then $A_x < A_y$, as it is, indeed, experimentally found.

Best calculations using a full diagonalization of spin-orbit interaction within crystal-field and charge-transfer states, as explained in Ref. 19, give for Ni^+(III): $A_y - A_x = 3.6\times10^{-4}$ cm^{-1}, which is not far from the experimental value, $A_y - A_x = 5\times10^{-4}$ cm^{-1} found for $CsCaF_3$:Ni^+(III). It is worth recalling here that, at variance with what is found for parameters like Δ_1, A_s, or $g_\parallel - g_0$, the MO coefficients such as β_0^2 are nearly independent of R_{eq}. The microscopic origin of this behavior is discussed in Ref. 15.

Having in mind Eq. (15), we can now understand the difficulties in detecting an orthorhombic character in d^9 complexes involving a ligand such as Cl^-. In fact, $A_p^0 = 463\times10^{-4}$ cm^{-1} for free F^-, while the corresponding quantity for Cl^- is equal only to 45×10^{-4} cm^{-1} and so the differences between A_y and A_x would be of the order of 0.1×10^{-4} cm^{-1}. Electron-nuclear double resonance (ENDOR) measurements would be able, however, to resolve such a small difference.

We will give now a qualitative discussion about the interaction with the two axial fluorines. As we have said, the ground state of a Ni^+ ion in an elongated octahedral environment is the $|x^2-y^2\rangle$. The first excited state is the $|3z^2-r^2\rangle$ but it is not coupled to the ground state by spin orbit. The $|xy\rangle$, $|xz\rangle$, and $|yz\rangle$ states that are mixed with the $|x^2-y^2\rangle$ by spin-orbit coupling are separated from the ground state by the cubic field splitting and so they have a small influence on the SHF parameters. However, the $|x^2-y^2\rangle$ state only forms "s" bonds with the four equatorial fluorines and consequently only the interaction with these four fluorines should be observed, while the experiments show the interaction with six fluorines. This problem was analyzed by O'Brien some years ago[23] and she concluded that the E_g JT mode of the NiF_6^{5-} complex could couple the $|x^2-y^2\rangle$ and $|3z^2-r^2\rangle$ states and the observed SHF interaction with the axial fluorines should come from the contribution of the $|3z^2-r^2\rangle$ orbital. However, taking into account that $A'_\parallel = A'_s + 2A'_p$ and $A'_\perp = A'_s - A'_p$, the experimental values of $|A'_\parallel|$ (6×10^{-4} cm^{-1}) and $|A'_\perp|$ (10×10^{-4} cm^{-1}) can only be obtained if $A'_s/A'_p < 0$ and this is not possible if we apply the O'Brien mechanism because the mixture with the $|3z^2-r^2\rangle$ orbital will give positive values for both A'_s and A'_p. In order to explain our results as well as those corresponding to other Ni^+ ions in elongated octahedral environments, we suggest that the spin polarization of the filled valence orbitals, mainly those with A_{1g} symmetry that give rise to a strong contribution to the SHF interactions with the axial fluorines, should be taken into account. A similar mechanism has been proposed to explain the isotropic part of the SHF structure of Cr^{3+} in some fluoroperovskites.[24] The spin polarization will likely give a negative A'_s value as well as a negative contribution to A'_p that will be overcome by the positive dipolar term.

Finally we want to comment on the thermal evolution of Ni^+ EPR signals. The signal of Ni^+(II) and Ni^+(III) disappear at about 300 K with a simultaneous decrease of all the lines. This can be associated with a decrease of the longitudinal relaxation time T_1. By contrast, in the Ni^+(I) spectrum different features are observed. In fact, the signal disappears at much lower temperature ($\sim$35 K). Besides, in the range 20–30 K the odd lines of the spectrum corresponding to centers with the axes perpendicular to the magnetic field broaden much faster than the even lines (Fig. 4). Both features can reasonably be explained as a result of the JT effect which is present only in the center I. Dynamical JT effects of Ni^+ centers have been previously reported[7,25] T_1 can depend on both the relaxation time T_{1R} corresponding to the reorientation of the centers among three quasiequivalent JT tetragonal distortions and the spin-lattice relaxation time T_{sl} that is present even if the reorientation is absent. This time T_{sl} can be strongly influenced by the peculiar structure of vibrational levels associated with a JT system and can be shorter than that corresponding to true (non-JT) tetragonal systems. On the other hand, associated with each of the lines is a frequency given by $\hbar\omega = \beta_e g_\perp B$ (where B gives the position of the line in the EPR spectrum), the reorientation alone would give rise first to a broadening of the lines which reach a different frequency after a jump to another quasiequivalent configuration. If the line frequency changes from ω_a to ω_b because of the jump, the broadening that appears if $\omega_a \neq \omega_b$ comes when[26,27]

$$(\omega_a - \omega_b)\tau \sim 1 , \quad (16)$$

where τ is the reorientation time. The dependence of τ on temperature is usually of the form

$$\tau = \tau_0 \exp(\Delta/KT) , \quad (17)$$

where Δ is the barrier to be overcome between quasiequivalent configurations. Therefore, increasing the temperature favors a decrease of τ and thus, the appearance of motional averaging, provided T_{sl} itself does not change in the same temperature range. Having these

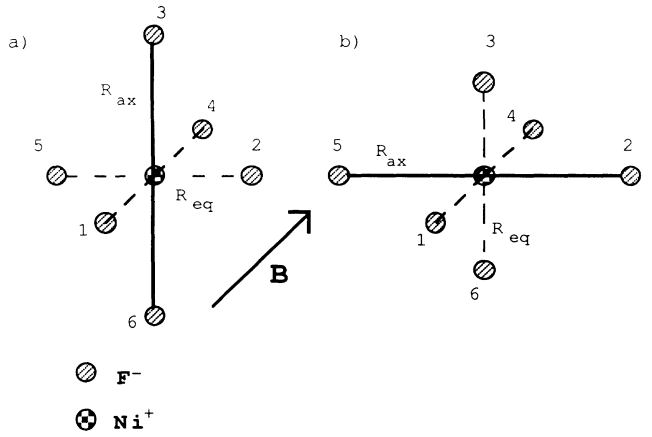

FIG. 6. The two Ni^+(I) Jahn-Teller configurations with the C_4 axis perpendicular to the applied magnetic field **B**.

ideas in mind the selective broadening and disappearance of odd SHF lines can be explained through the reorientation between the two JT configurations displayed in Fig. 6. In fact, the frequency of a SHF line given in the configuration 6(a) by

$$\hbar\omega_a=\beta_e g_\perp B + A_\parallel(M_1+M_4)+A_\perp(M_2+M_5) + A'_\perp(M_3+M_6)\ , \tag{18}$$

where M_i is the I_z value for the i-F^- nucleus (see Fig. 6), becomes

$$\hbar\omega_b=\beta_e g_\perp B + A_\parallel(M_1+M_4)+A'_\perp(M_2+M_5) + A_\perp(M_3+M_6) \tag{19}$$

in the configuration 6(b). Therefore,

$$\hbar(\omega_a-\omega_b)=(A_\perp-A'_\perp)[(M_2+M_5)-(M_3+M_6)]\ . \tag{20}$$

If $M_2+M_5=M_3+M_6$, $\omega_a=\omega_b$ and no broadening of these lines due to reorientation is expected. That condition is fulfilled by the even lines in our spectrum (and not by the odd ones) and so, we expect a smaller broadening for them, in agreement with the experimental results. The same analysis has been applied to other lines besides the seven main ones, and the results seem to be in agreement with the experiments although the low intensity of those other lines and the overlapping problems precludes us from making a more detailed study.

In order to get a rough estimation of the parameters τ_0 and Δ, we have assumed that at 30 K, the condition given by Eq. (16) is fulfilled while at 20 K, where a "static" spectrum is still seen, τ (20 K)$\cong 10\tau$(30 K). From the last condition, a value of $\Delta\cong 100\ cm^{-1}$ is estimated. Taking, in Eq. (20), $A_\perp=25\times10^{-4}\ cm^{-1}$, $A'_\perp=-10\times10^{-4}\ cm^{-1}$ (as obtained from the signs of A'_s and A'_p) $|M_2+M_5-M_3-M_6|=2$, the maximum jump $\hbar(\omega_a-\omega_b)$ becomes equal to $70\times10^{-4}\ cm^{-1}$ and thus, using Eq. (16), a value of $\tau_0\cong10^{-11}$ s is reached. The present estimation of τ_0 and Δ give rise to values lying in the same range as those observed in other d^9 JT systems.[28,29]

ACKNOWLEDGMENTS

This work has been supported by the CICYT under Project Nos. MAT 92-1279 and PB 92-0505.

[1]J. Ferguson, H. J. Guggenheim, and D L. Wood, J. Chem. Phys. **40**, 822 (1964).
[2]J. E. Ralph and M. G. Townsend, J. Phys. C **3**, 8 (1970).
[3]M. E. Vehse, K. H. Lee, S. I. Yun, and W. A. Sibley, J. Lumin. **10**, 149 (1975).
[4]P. J. Alonso, R. Alcalá, and J. M. Spaeth, Phys. Rev. B **41**, 10 902 (1990).
[5]S. A. Payne, Phys. Rev. B **41**, 6109 (1990).
[6]H. Bill, in *The Dynamical Jahn-Teller Effect in Localized Systems* (North-Holland, Amsterdam, 1984).
[7]W. Hayes and J. Wilkens, Proc. R. Soc. London, Ser. A **281**, 340 (1964).
[8]E. Zorita, P. J. Alonso, and R. Alcalá, Phys. Rev. B **35**, 3116 (1987).
[9]R. Alcalá, E. Zorita, and P. J. Alonso, Phys. Rev. B **38**, 11 156 (1988).
[10]M. T. Barriuso, J. A. Aramburu, and M. Morreno, J. Phys. Condens. Matter **2**, 771 (1990).
[11]G. M. Nurullin, L. N. Galygo, A. V. Egranov, and A. I. Nepomnyachikh, J. Phys. Condens. Matter **3**, 83 (1991).
[12]M. T. Barriuso and M. Moreno, Solid State Commun. **51**, 335 (1984).
[13]R. Alcalá, E. Zorita, and P. J. Alonso, J. Phys. C **21**, 461 (1988).
[14]M. Moreno, M. T. Barriuso, and J. A. Aramburu, Appl. Magn. Reson. **3**, 283 (1992).
[15]J. A. Aramburu, M. Moreno, and M. T. Barriuso, J. Phys. Condens. Matter **4**, 9089 (1992).
[16]A. Abragam and B. Bleaney, *Electron Paramagnetic Resonance of Transition Ions* (Clarendon, Oxford, 1970).
[17]K. H. Johnson, Adv. Quantum Chem. **7**, 143 (1993).
[18]J. H. Ammeter, A. B. Burgi, J. C. Thibeault, and R. Hoffmann, J. Am. Chem. Soc. **100**, 3686 (1978).
[19]J. A. Aramburu and M. Moreno, J. Chem. Phys. **83**, 6071 (1985).
[20]E. Clementi and C. Roetti, At. Data Nucl. Data Tables **14**, 177 (1974).
[21]G. Fernández-Rodrigo, M. Flórez, L. Pueyo, M. Moreno, and M. T. Barriuso, Cryst. Lattice Defects **16**, 281 (1987).
[22]J. A. Aramburu and M. Moreno, Solid State Commun. **62**, 513 (1987).
[23]M. C. O'Brien, Proc. R. Soc. London, Ser. A **281**, 323 (1964).
[24]M.E. Ziaei, Ph.D. thesis, Oxford University, 1977.
[25]A. Shoenberg, J. T. Suss, Z. Luz, and W. Low, Phys. Rev. B **9**, 2047 (1974).
[26]G. K. Fraenkel, J. Chem. Phys. **42**, 4275 (1965).
[27]G. K. Fraenkel, J. Phys. Chem. **71**, 134 (1967).
[28]B. L. Silver and D. Getz, J. Chem. Phys. **61**, 638 (1974).
[29]D. H. Powell, L. Helm, and A. E. Merbach, J. Chem. Phys. **95**, 9258 (1991).